Electron Spin Resonance Study of Radical Formation in *cis*-Poly(phenylacetylene)/Ferric Acetylacetonate–Triethylaluminum (PPA/Fe–Al). 2. Results and Interpretation

A. Langner*,† and P. Ehrlich

Department of Chemical Engineering, State University of New York at Buffalo, Buffalo, New York 14260. *Received August 15, 1989*

ABSTRACT: The line-shape and saturation analysis for inhomogeneously broadened ESR spectra, developed in the previous paper, is used to study the change of the PPA/Fe–Al resonance signal with temperature and polymer aging. A mechanism for radical formation, involving backbone cyclization reactions, is proposed to interpret the irreversible increase in spin concentration observed above −70 °C. As before, the spectra of the soluble and insoluble fractions of the polymer are interpreted as arising largely from triphenylcyclohexadienyl radicals formed upon cyclization of a cis-cisoid hexatriene precursor. An analysis of the resonance signal of the catalyst revealed that a low Al:Fe ratio at the active polymerization site leads to a high concentration of the cis-cisoid conformation. The presence of oxygen-complexed radicals with shorter spin–lattice relaxation times is inferred from saturation experiments.

Introduction

A form of poly(phenylacetylene) (PPA) that is rich in the cis isomer can be made in the presence of a ferric acetylacetonate/triethylaluminum catalyst (PPA/Fe–Al).[1,2] It contains a crystalline component that melts at about 120 °C and displays a distinct resonance Raman[3] and fluorescence[4] spectrum that we have attributed to the cis-cisoid helical conformation.[2] The crystalline fraction can be purified by treating the polymer with chloroform, which extracts the noncrystalline, soluble fraction of *cis*-PPA.[4] The two fractions display different ESR spectra, which also differ from spectra reported in earlier studies.[5,6] Preliminary investigations, employing a line shape and saturation treatment for inhomogeneously broadened spectra,[7] suggested that the source of these resonance signals was the triphenylcyclohexadienyl (TPCH) radical,[8] formed in the course of backbone-cyclization reactions.[9] Previous thermal stability studies of the cis isomer had shown that the spin concentration of the polymer increases irreversibly at elevated temperatures, peaking near 120 °C.[5] Recently, it was shown that the polymer is also unstable at room temperature.[10]

We have applied the line shape and saturation treatment of the previous paper, paper 1, to obtain a quantitative description of the temperature dependence and time evolution of the resonance signals of the various radical species found in this polymer. This enabled us to make a clearer separation and identification of the polymer and catalyst signals and to resolve a further component of the polymer signal, believed to be an oxygenated radical.

Experimental Procedure

All ESR experiments were performed on a Varian E-104 spectrometer with an E-231 multipurpose resonance cavity, operated in the TE_{102} mode. Operation was in the X-band, nominally 9.07 GHz, with 100-kHz field modulation for phase-lock detection (i.e., signals were recorded in the first-derivative mode). Sample tubes were placed into a quartz Dewar (11.5-mm o.d., 6-mm i.d.), which occupied the central axis of the cavity, mutually perpendicular to the long axis and magnetic-field directions of the cavity. The Dewar allowed the performance of variable-temperature experiments, which were executed with a Varian E-257 variable-temperature controller using prepurified-grade nitrogen as a carrier gas.

The E-104 spectrometer has no facility for externally biasing the signal detector into the linear regime (i.e., signal intensity is proportional to the square root of the incident power). Therefore, we had to calibrate the spectrometer to account for detector nonlinearities and for the degree of undercoupling of the waveguide to the resonance cavity. The power-independent signal, I'_R, was found to have the form

$$I'_R = \frac{y' G_x}{P_w^{n} r^{(2n-1)}(1-r^2) G_s} \tag{1}$$

where y' is the recorded signal height, G_x is the crystal detector gain factor, P_w is the power in the waveguide as measured by an HP-432A power meter connected to an HP-X486A thermister, n ($1 \geq n \geq 0.5$) gives the dependence of the detector response on the incident power, r is the reflection coefficient of the cavity, and G_s incorporates the effects of signal gain and field modulation amplitude.

ESR spectra were recorded for absorption, χ'', signals. Great care was exercised to avoid modulation and fast-passage distortions to the line shapes.

To obtain quantitative results from saturation experiments we had to determine the relation between the microwave power coupled into the resonance cavity, P_c, and the power in the magnetic component of the microwave field at the sample. Using the analysis of Poole[11] we have determined that $\langle H_1^2 \rangle_s = 2.602 P_c = H_1^2{}_{max}/2$, where the magnetic field, H_1, is given in gauss and the power is given in watts. It has been shown by Singer et al.[12] that a quartz Dewar intensifies the field at the sample. We observed an enhancement of 3.4 times the empty cavity value, making the average power in the field at the sample $\langle H_1^2 \rangle_s = 8.85 P_c$. We have assumed the relation between the sample-average and the maximum field, given above, to hold.

Absolute spin concentrations were determined by comparison to the Varian 0.1% strong pitch in a KCl standard, rated at 3×10^{15} spin/cm (±30%). g factors were determined by comparison to polycrystalline diphenyl picrylhydrazyl (DPPH), $g = 2.0036$. The latter was also employed to test the power calibration procedure.

The samples investigated in this study were derived from three different polymerization batches, here indicated as M7, M8, and N1. All polymerizations were run at room temperature in tetralin. The molar ratios of monomer to triethylaluminum to ferric acetylacetonate for the three batches were

† Present address: Department of Chemistry, Rochester Institute of Technology, Rochester, NY 14623.

0024-9297/90/2223-2203$02.50/0

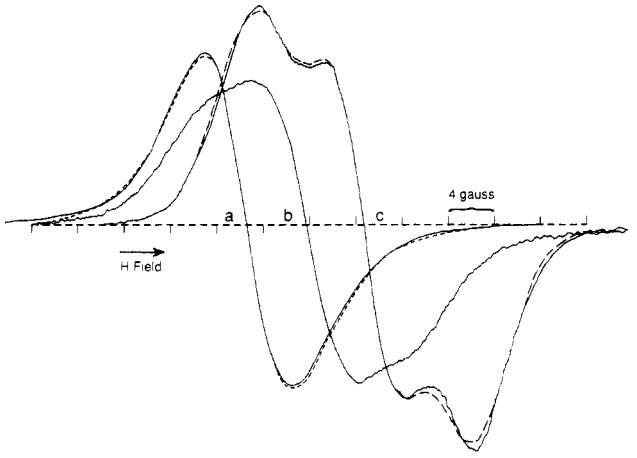

Figure 1. ESR spectra of the polymer radicals in *cis*-PPA/Fe–Al. (a) Soluble fraction, g = 2.0028; (b) unfractionated polymer, g = 2.0027; (c) insoluble fraction, g = 2.0026. Solid lines are experimental spectra. Dashed lines are best-fit theoretical curves (see text).

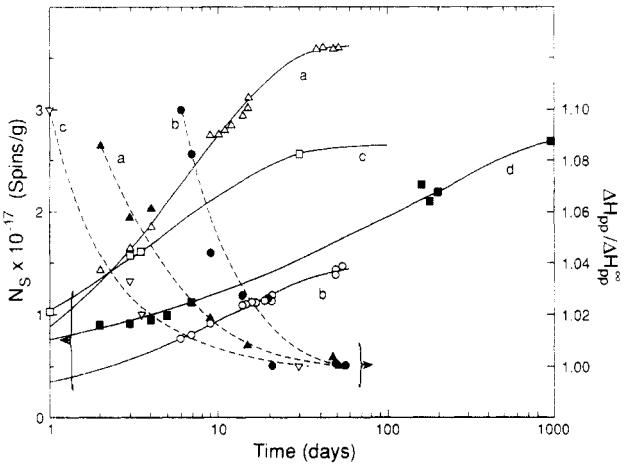

Figure 2. Time evolution of the spin concentration, N_S, and the line width, ΔH_{pp}, for the polymer radicals of *cis*-PPA/Fe–Al. The given line width is measured with respect to its long-time asymptotic limit ΔH_{pp}^{∞}. (a) Insoluble fraction from batch M7; (b) soluble fraction from batch M7; (c) soluble fraction from batch N1, stored in $CHCl_3$ solution; (d) soluble fraction from batch N1, stored as a powder. Dashed lines are added as a guide. Solid lines are best-fit curves for the kinetic model (see text).

81.86:2.49:1 (M7), 119.65:4.98:1 (N1), and 119.65:9.96:1 (M8). All samples were washed with methanol and 0.1 N HCl (1.0 N for N1). Batch M7 was also left to sit in pure methanol for 2 weeks after the initial washings. Batches M8 and N1 were brick red, coarse, granular powders. Batch M7 was bright red with finer granules.

Each batch was separated into a chloroform-soluble and a chloroform-insoluble fraction by a procedure described elsewhere.[13] The latter fraction contained the insoluble crystalline polymer referred to in the Introduction. All samples, from the onset of polymerization through the course of the ESR experiments, were stored in the dark, since light had been shown capable of increasing the spin concentration.[14] Samples were stored and treated in air except when in evacuated sample tubes, where they were under 0.2 torr of nitrogen.

ESR measurements were performed on powder samples of the soluble and insoluble fractions. The insoluble fraction, if very pure, was a deep maroon color and when containing residual soluble polymer was brick red. The soluble fraction gave a yellow-brown, somewhat statically charged powder and yellow solutions.

For both low- and high-temperature operation 10–20 min were allowed for thermal equilbration of the sample at a given temperature level. Temperatures for cooling runs were changed by 10 °C increments. For high-temperature experiments, samples were annealed for 24–36 h in an oil bath prior to recording the ESR spectrum.

Experimental Results

A. General Characteristics of the Polymer Spectrum. Representative room temperature spectra of $CHCl_3$-soluble and $CHCl_3$-insoluble fractions and of the unfractionated polymer are shown in Figure 1. Signals from the soluble fraction exhibit a single, slightly asymmetric line at g = 2.0028 and line width ΔH_{pp} = 8 G; those from the insoluble fraction give a partially resolved, slightly asymmetric quartet with the outer peaks separated by ΔH_{pp} = 18 G and the line center at g = 2.0026. The spectra from the unfractionated polymer[5] can be deconvoluted into these two signal types, with ratios 2:3 and 3:2 for batches M7 and M8, respectively.

Figure 2 shows typical results for the time evolution of the spin concentration, N_s, and of ΔH_{pp} for $CHCl_3$-insoluble (curve a) and $CHCl_3$-soluble (curves b–d) samples. The spin concentrations for the unfractionated polymers were (1.5–1.7) × 10^{16} spins/g. The increase of N_s since the time at which the samples were dried (t = 0) is much greater for insoluble than soluble fractions; both experience a decrease in ΔH_{pp} with time. Both of these changes indicate a prolonged process of radical generation at room temperature in the solid state, a process that is most rapid in the freshly dried polymer but that still proceeds after several months. Figure 2 also contrasts the time evolution of N_s for two freshly dried samples of soluble polymer (curves c and d), one of which, c, had been kept in chloroform solution for several months prior to removal of the diluent and drying. The sample that had been kept in chloroform displays no increase in N_s during that time, but, immediately after drying, N_s increases rapidly, overtaking that of the sample that had not experienced a prior prolonged exposure to chloroform. Evidently the process of radical generation depicted by Figure 2 does not take place, or is greatly slowed, in chloroform solution, but this treatment conditions the polymer for rapid radical generation to a very high level after drying. We shall later suggest (see Discussion) that the precursor to radical formation is, in fact, the cis-cisoidal helical conformer, and that it is generated in solution.

The low-temperature behavior (−128 to 22 °C) of the signal intensity for freshly cast and aged films made from the insoluble fraction is depicted in Figure 3. Unlike the aged sample, the relatively unaged sample displays a marked non-Curie temperature dependence ($\chi(T) \neq \text{const}\cdot T^{-1}$) as well as an irreversible signal increase above −70 °C. Results for the $CHCl_3$-soluble fraction are similar.

The high-temperature behavior (22 to 200 °C) of N_s was qualitatively similar to that reported by Holob et al.[5] for unfractionated polymer, showing an increase with increasing temperature up to 120 °C. Above this temperature, thought to be the melting point of the helix,[4] N_s and ΔH_{pp} decreased sharply for oxygen-doped material; however, they remain constant at N_s = 10^{19} spins/g and ΔH_{pp} = 15 G for samples determined to have a very low oxygen content. The former behavior was observed in Holob's studies.[5]

Representative saturation plots, for soluble and insoluble fractions are given in Figures 4 and 5. We have plotted the power dependences of the signal height, V'_R, the peak-to-peak width, and the quantity $I'_R = V'_R/P^{1/2}$, where P is the incident power on the sample. I'_R should attain a constant value, I'_{R0}, which is proportional to the

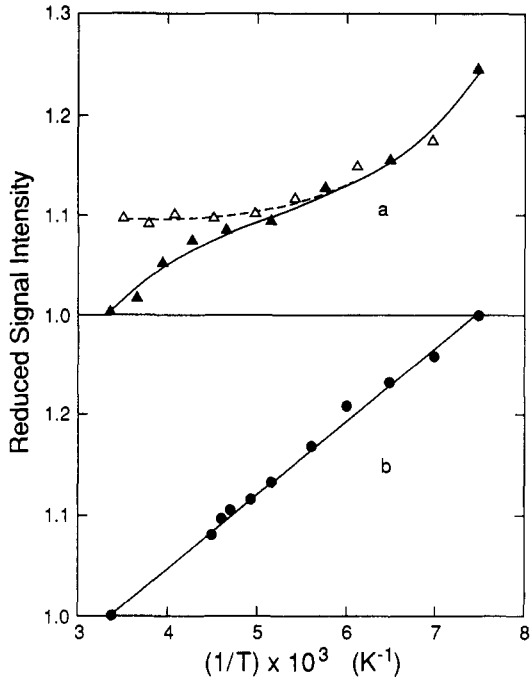

Figure 3. Low-temperature study of the signal intensity of the polymer radicals for the insoluble fraction. Solid symbols represent cooling. Open symbols represent heating: (a) fresh sample; (b) aged sample.

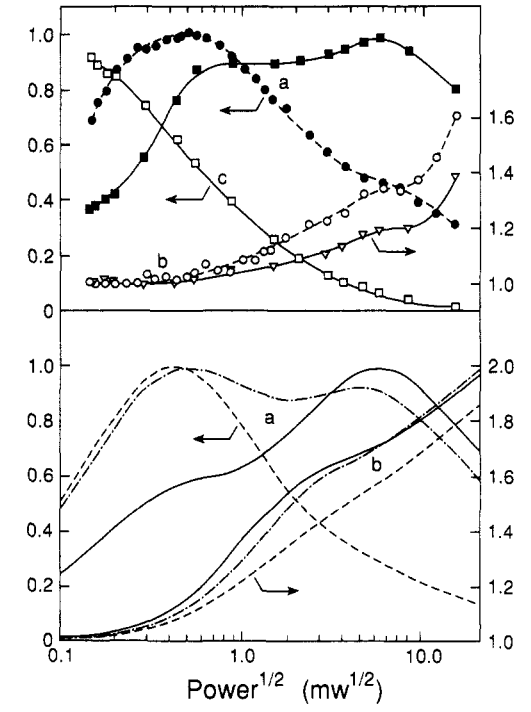

Figure 4. Experimental (upper) and theoretical (lower) saturation curves for the soluble fraction. (a) V'_R versus $P^{1/2}$ for a low Al:Fe ratio sample (●) and a high Al:Fe ratio sample (■). (b) $\Delta H_{pp}/\Delta H_{pp0}$ versus $P^{1/2}$ for a low Al:Fe ratio sample (○) and a high Al:Fe ratio sample (△). (c) Typical relation for I'_R/I'_{R0} versus $p^{1/2}$ (▽). Theoretical curves are for an "oxy" radical fraction of 0.3 (—), 0.15 (- · -), and 0.03 (- -).

spin concentration, at sufficiently low power levels. A common feature of all the saturation curves recorded is the failure to reach this limiting value as can be seen on Figure 4. Consequently we must resort to the methods of paper 1 to obtain reliable values of spin concentrations and characteristic spectral parameters. The results show that for samples with a large Al/Fe ratio the V'_R curve is bimodal. In the low Al/Fe samples, the high-

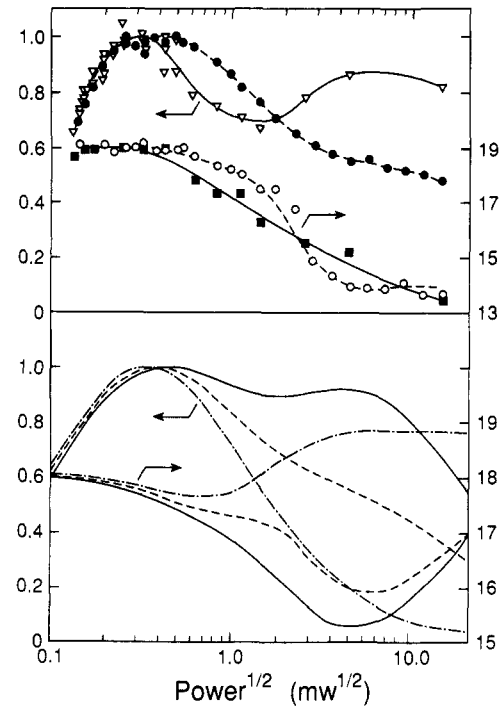

Figure 5. Experimental (upper) and theoretical (lower) saturation curves for the insoluble fraction. (a) V'_R versus $p^{1/2}$ for a low Al:Fe ratio sample (●) and a high Al:Fe ratio sample (△). (b) $\Delta H_{pp}/\Delta H_{pp0}$ for a low Al:Fe ratio sample (○) and a high Al:Fe ratio sample (■). Theoretical curves are for an "oxy" radical fraction of 0 (- · -), 0.03 (- - -), and 0.06 (—).

power peak is replaced by a shoulder. Lastly, the line widths of the insoluble samples become narrower with increasing power, while the line widths of the soluble samples broaden.

B. Line-Shape and Saturation Analysis. Spectra and saturation curves, recorded over a broad range of temperatures and sample ages, were analyzed by the line-shape model and regression procedure described in paper 1. To enable us to quantify the results of a large array of experiments, we restrict our analysis to testing the hypothesis that, aside from catalyst residues, which will be discussed in the next section, the polymer contains three different radical types: (1) triphenylcyclohexadienyl radicals (TPCH), (2) π-electron radicals delocalized over a segment of the conjugated polymer chain, to be referred to as chain radicals, and (3) π-electron radicals complexed by either a hydroxy or a peroxy group, to be referred to as oxy radicals. All radical types are considered to be nonmobile, although they are delocalized over several carbon centers. The spatial extent of the delocalization, and consequently the line width, depends on the degree of planarity of the chain carbons with each other and with the cyclohexadienyl ring. The degree of planarity will be distributed over a range of values. As a result we anticipate an inhomogeneously broadened line with a Curie temperature dependence, resulting from multiple hyperfine interactions. The experimental signatures for the three radical types can be seen in the spectra of the insoluble fraction and the soluble fraction and the high-power mode of the saturation curves, respectively.

The chain radical is expected to give a featureless resonance signal, which is characteristic of most conjugated polymers. It can be demonstrated by simple quantum chemical methods that the TPCH radical will exhibit two dominant hyperfine splittings, proportional to the ortho- and para-hydrogen splittings of the cyclohexadiene radical, 9 and 13.4 G, respectively.[15] These hyperfine cou-

Table I
Regression Results for Soluble *cis*-PPA

sample[a]	age,[b] days	temp, K	$\alpha\tau_0$[c]	σ_0, G	T_1, 10^{-4} s	T_2, 10^{-7} s	$(N_s)_T$,[d] 10^{16}	N_{oxy}[e]/$(N_s)_T$
8-1	13	294	0.326	6.91	0.74	3.5	2.64	0.39
8-1	19	294	0.517	6.78	0.58	2.3	2.97	0.18
8-2	33	294	0.192	7.07	3.2	5.9	4.61	0.18
8-2	49	294	0.310	7.14	3.2	3.6	7.51	0.30
8-2	262	223	0.522	6.85	3.7	2.2	15.6	0.24
8-2	267	294	0.618	6.43	3.2	2.0	13.5	0.23
8-2	263	173	0.670	6.70	1.6	1.8	27.0	0.21
7-1	6	294	0.632	5.85	25.	2.2	9.97	0.07
7-1	52	294	0.700	5.35	25.	2.1	15.6	0.05
7-1	52	133	0.557	5.36	35.	2.7	34.5	0.05
1-1	3	294	0.312	6.46	2.4	4.0	4.82	0.37
1-1	179	294	0.288	7.35	1.3	3.8	18.5	0.23
1-1	954	294	0.140	8.21	1.8	7.0	25.6	0.20
1-2	4	294	0.280	6.17	1.6	4.6	6.94	0.17
1-2	30	294	0.420	5.70	1.6	3.4	18.8	0.07

[a] The sample designation *M*-*N* refers to the *N*th sample of polymerization batch *M*: *M* = 1, batch N1; *M* = 7, batch M7; *M* = 8, batch M8. [b] The sample is considered to be of 0 age at the time the sample has been dried. [c] $\alpha\tau_0$ is the value for the unsaturated spectrum and not that obtained by regression of the line shape alone (refer to paper 1). [d] N_s = total spin concentration in spins per gram. [e] N_{oxy} = spin concentration in spins per gram for oxygen-trapped radicals.

Table II
Regression Results for Insoluble *cis*-PPA[a]

sample	age, days	temp, K	$\alpha\tau_0$	σ_G, G	A_1,[b] G	A_2, G	T_1, 10^{-4} s	T_2, 10^{-8} s	$(N_s)_T$, 10^{16}	$N_{oxy}/(N_s)_T$
oxy[c]	246	273	0.180	12.92				3.5	473.6	0.91
8-3	6	294	0.256	5.62	5.41	7.92	10.0	5.6	18.4	0.12
8-3	24	294	0.282	5.52	5.42	7.79	10.0	5.1	21.7	0.08
8-3	104	294	0.285	5.60	5.37	7.77	10.0	5.0	26.3	0.09
8-3	246	288	0.356	5.44	5.28	7.61	10.0	4.2	43.4	0.06
8-3	134	130	0.286	5.42	5.31	7.52	29.0	5.2	59.7	0.09
8-4	21	294	0.231	5.96	5.72	7.63	10.0	5.8	9.72	0.212
8-4	246	294	0.365	5.69	5.45	7.29	10.0	3.9	22.5	0.09
8-4	267	294	0.354	5.69	5.46	7.36	10.0	4.0	21.7	0.11
8-4	263	128	0.409	5.40	5.52	7.06	29.0	3.6	50.0	0.11
7-2	7	294	0.168	6.19	5.86	7.59	6.0	7.7	20.7	0.04
7-2	21	294	0.484	5.49	5.66	7.27	6.0	3.0	35.5	0.02
7-2	54	294	0.442	5.49	5.53	7.31	6.0	3.2	69.9	0.01
7-2	54	133	0.334	5.20	5.71	6.88	53.0	4.3	115.0	0.01

[a] Refer to Table I for definitions. [b] A_1 and A_2 are the ortho- and para-hydrogen hyperfine coupling constants for the TPCH radical. [c] Insoluble *cis*-PPA sample after oxygen doping.

plings were included in the regression analysis of the spectra from samples of the insoluble fraction. An approximation to the line shape of the oxygen-trapped radical was obtained from the spectrum of a heavily oxygen-doped sample; it is a nearly Gaussian line with ΔH_{pp} = 13 gauss and g = 2.0029. Previous investigations of *cis*-PPA revealed similar spectra.[5,6]

Typical regression fits of the spectra of the soluble and insoluble fractions are given in Figure 1; agreement is very good. The spectra of the insoluble fraction was modeled by the superposition of resonance line shapes resulting from two different hyperfine couplings, 5.5 and 7.5 G. Inclusion of the "oxy" radical in the parameter set for the regression did not lead to a statistically significant improvement in the regression fit. The spectrum of the soluble fraction was modeled as the superposition of two resonance line shapes centered at g = 2.0026 and 2.0029. Only the line shape of the majority species, the chain radical, could be optimized, the regression analysis being very insensitive to small changes in the functionality of the signal of the oxy radical.

Although the line-shape analysis was rather insensitive to the presence of the "oxy" radical, its concentration could be determined quite accurately by analyzing the saturation curves. Theoretical curves corresponding to the experimental data presented in the previous section are given in Figures 4 and 5 for the soluble and insoluble samples, respectively. It should be noted that the exclusion of the "oxy" signal in the analysis of signals of the insoluble fraction always leads to a line-width broadening at high powers. Inclusion of a small percentage of "oxy" signal, which saturates at higher powers, models the observed narrowing quite well. The curves of signal height versus power, V'_R versus $P^{1/2}$, are extremely sensitive to the concentration of the "oxy" radical, particularly for the insoluble fraction, enabling us to make good estimates of its value. The results of the combined regression and saturation analyses are given in Tables I and II for the soluble and insoluble fractions, respectively. Aside from the obvious difference in the resolution of the hyperfine splittings, the soluble fraction displays certain differences from the insoluble one: (1) Total spin concentrations are three to four times smaller. (2) The ratio N_{oxy}/N_s is larger, though N_{oxy} is comparable in the two fractions. (3) Values of the Gaussian envelope width, σ_G, are 20–30% larger; they decrease with aging but increase at higher temperatures. (4) The spin–lattice relaxation time, T_1, of the soluble fraction, (1–3) × 10^{-4} s, is smaller than that of the insoluble fraction, (6–1) × 10^{-3} s; due to approximations invoked in our analysis a similar comparison cannot be made for T_1 of the "oxy" radicals, which, however, can be estimated to be approximately 10^{-6} s. For the insoluble fraction, the regressed hyperfine coupling constants decrease with sample aging. The soluble fraction which was stored in chloroform solution exhibits behavior intermediate between that of the soluble and insoluble fractions.

C. Analysis of the Catalyst Signal. The resonance lines of the polymer radicals are superimposed on a broad, unsaturable signal attributable to various Fe^{3+} species

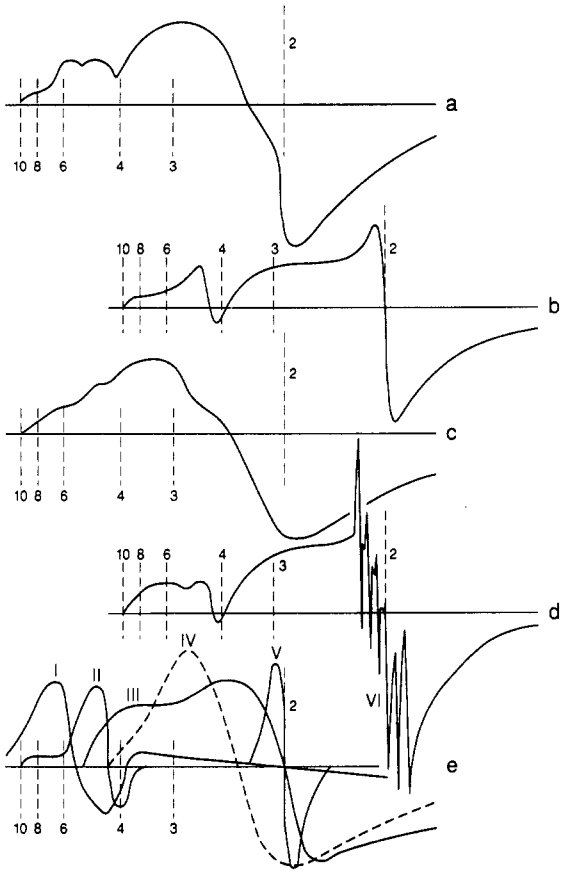

Figure 6. ESR spectra of the Fe–Al catalyst system. Signals not attributable to the Fe–Al complex have been subtracted out. (a) Soluble fraction of batch M7; Al:Fe = 2.5:1. (b) Soluble fraction of batch M8; Al:Fe = 10:1. (c) Insoluble fraction of batch M7. (d) Insoluble fraction of batch M8. (e) Resonance line shapes of which spectra a–d are a convolution.

of the $Fe(AcAc)_3/AlEt_3$ catalyst system.[8] The strength and characteristics of the catalyst signal vary considerably between spectra of the soluble and the insoluble fraction of a given polymerization batch as well as among the three batches studied, with Al-to-Fe ratios of 10:1, 5:1, and 2.5:1 respectively. In Ziegler–Natta polymerization the role of the group III metal, Al, is to reduce the transition metal, Fe, and regulate the rate and stereospecificity of the reaction.[16] It is therefore of interest to identify the characteristics of the catalyst site that favor the formation of cis-cisoid, i.e., helical sequences. Since the focus of this paper is the chain radical and its precurser, we present only the results of our analysis. (For details see ref 10.)

Representative powder spectra of the catalyst signal for the various polymer fractions are given on Figure 6. Modeling work, performed on spectra recorded between 128 and 400 K, revealed that these resonance lines can be deconvoluted into the six line shape types designated on Figure 6e. Types I, II, and V, centered at $g = 6$, 4.37, and 2.007, respectively, exhibit a nearly Curie ($1/T$) temperature dependence for $T < 180$ °C, indicative of isotropic transitions. The other signal types behave like powder spectra from orientation-dependent transitions among spin states whose energies are determined by local electric fields (i.e., Stark effect).[17] The sextet signal set, type VI, observed only for the insoluble fraction of the polymer produced with a high Al-to-Fe ratio catalyst system, undergoes a large increase with increasing temperature up to 90 °C. However, it decreases rapidly and irreversibly above 120 °C, the melting point of the crystalline form of the polymer.[4]

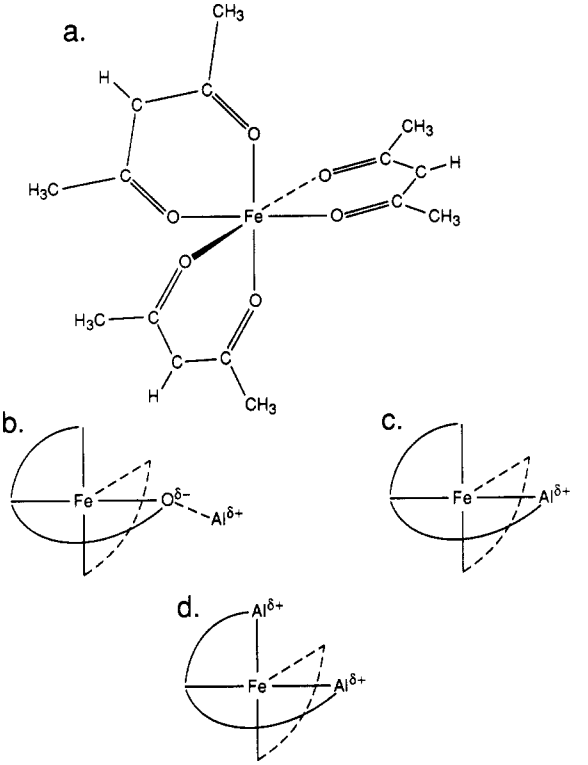

Figure 7. Structures of the $Fe(AcAc)_3/AlEt_3$ catalyst system. (a) Pure $Fe(AcAc)_3$. (b) Weak Fe–Al coupling. (c) Strongly coupled axial complex. (d) Strongly coupled orthorhombic complex.

The various signal types depicted on Figure 6e are signatures for the different iron–aluminum complexes presented in Figure 7. Pure ferric acetylacetonate (Figure 7a) consists of three chelating acetylacetonate anions whose carbonyl oxygens are bonded to the central Fe^{3+} ion in an octahedral complex.[18] The ESR spectrum of $Fe(AcAc)_3$ is similar to signal type IV. For weakly bound aluminum, as is represented in Figure 7b, all five transitions between the pure spin states of the $S = 5/2$ ion are observable; however, only the $-(1/2)$ to $1/2$ transition is isotropic (type V) and consequently discernable from the powder spectra of the other four orientation-dependent transitions (type III). For stronger complexation by aluminum, either in an axial (Figure 7c) or an orthorhombic (Figure 7d) configuration, the $S = 5/2$ spin states mix. The resulting transitions, type I and II, respectively, are very similar to those discussed by Sands[19] and Castner et al.[20] for Fe^{3+} in quartz glasses. The next level of interaction is a reduction of Fe^{3+} to Fe^{2+} by aluminum, resulting in a loss of the ESR signal.[21] This interaction is probably the cause of the small catalyst signals for samples with a high Al:Fe ratio. If the iron and aluminum centers are kept close together by steric hindrances, only partial charge transfer from Fe to Al will be possible. This will result in a strong hyperfine interaction between the $I = 5/2$ nucleus of aluminum and the iron electronic spins. We propose that this is the origin of the sextet (type VI). This assignment is consistent with the observed signal decrease above 120 °C[10] and the absence of hyperfine structure in the spectra of the soluble fraction and samples with a small Al:Fe ratio. An alternate explanation that attributes this spectral feature to an Mn^{2+} ion seems invalid in light of this experimental evidence. Signal type VI represents the broadest Fe–Al hyperfine pattern recorded to date, being nearly 80 times wider than that reported for the lanthanide alums.[23]

From this description of the variation of the catalyst signal with polymer fraction, one concludes that the polymerization of phenylacetylene to a cis-cisoid-rich polymer is favored by a low Al:Fe ratio. This is consistent with the observation that the percentage of insoluble fraction is larger for the polymer grown at a low Al:Fe ratio. All the catalyst spectra from the soluble fractions were richer in signatures from a strongly complexed aluminum structure than their insoluble counterparts.

Discussion

We will propose a model for the microstructure of the polymer chain, the structure of the radical responsible for the main part of the polymer's ESR spectrum, and a reaction mechanism that is capable of accounting for the time evolution of the ESR signal.

The basic structure of PPA/Fe–Al may be viewed as that of a copolymer of cis-transoid and cis-cisoid units. It is believed that the latter are capable of forming a helix, which has been proposed as the structure of the insoluble, crystalline fraction of PPA/Fe–Al.[2,9,24] An examination of the NMR and fluorescence spectra of the soluble fraction indicated that they contained disordered chain segments, rich in cis-transoid units, as well as cis-cisoidal segments that must be long enough to stabilize the helical structure. In addition, a study of the phase equilibra of the unfractionated polymer in chloroform or in carbon tetrachloride indicated that the soluble fraction of PPA/Fe–Al is best described as a block copolymer of cis-transoid and cis-cisoid units.[4,13] The insoluble, crystalline fraction is then to be denoted as a somewhat impure homopolymer of cis-cisoid units containing cis-transoid impurities. At room temperature, in solution, there is a certain degree of intechange among these structures; the formation of cis-cisoid helices being favored in chloroform as evidenced by the gelation of the polymer maintained in solution for long periods of time.[10] As has been pointed out by Percec and Simionescu,[9] sequences of three connected cis-cisoid links can readily undergo cyclization reactions resulting in 1,3,5-triphenylcyclohexadienyl units in the chain. The cyclization reaction is quite facile in solution, having an activation energy, E_a, of only 71 kJ/mol.[9] As the polymer is dried, either from a swollen suspension or as an amorphous film, this cyclization is slowed considerably ($E_a \sim 126$ kJ/mol).[9]

It is proposed that the cyclization proceeds via an electrocyclization reaction in which a *cis*-1,3,5-hexatriene is converted to a 2,4-cyclohexadienyl ring by way of a benzene-like transition state, as depicted in Figure 8. The energy barrier of the reaction depends on whether the transition state is disrotatory (Hückel state) or conrotatory (Möbius state). The Hückel transition state has a lower energy than the Möbius state and should be the one participating in solution. Generation of the proposed 1,3,5-triphenylhexadienyl (TPCH) radical, which involves the loss of a hydrogen atom at the bonding carbon, is likely to proceed through the Möbius state, however. The solid polymer is conjectured to be subject to internal stresses caused by rapid solvent volatilization and can be thought of as being frozen into nonequilibrium configurations. If a cis-cisoid sequence becomes locked into a strained configuration it may cyclize to relieve excess energy. Occasionally, this cyclization could well be accompanied by a loss of a hydrogen atom from the chain-closure site resulting in a TPCH radical (Figure 8). We suggest that this is the major radical creation mechanism in the solid. In the soluble polymer fraction the highest TPCH radical concentration would then be

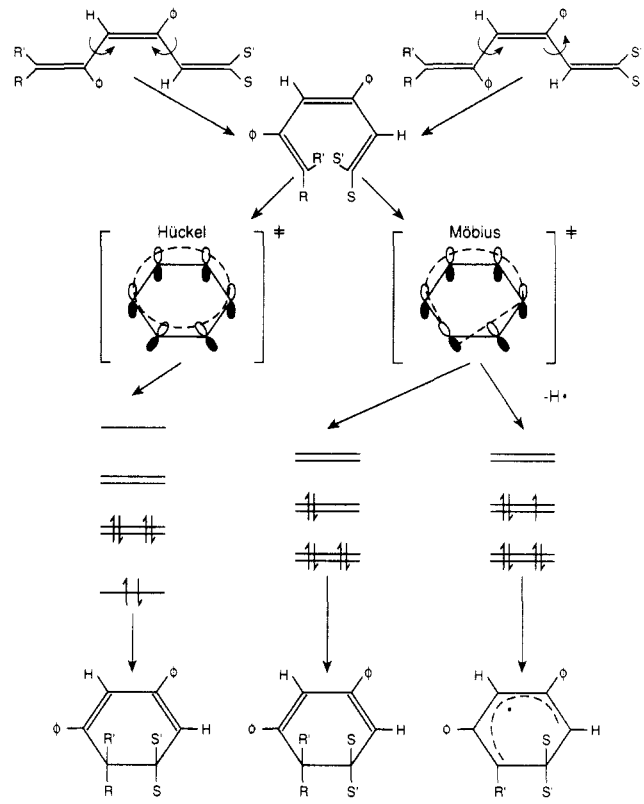

Figure 8. Electrocyclization reaction converts a cis-cisoid 1,3,5-hexatriene to a 2,4-cyclohexadiene. The reaction proceeds by either a low-energy, disrotary pathway with a Hückel transition state, or by a high-energy, conrotary pathway with a Möbius transition state. A hydrogen atom can be more readily lost from the latter transition complex resulting in a cyclohexadienyl radical.

generated by initial exposure of the polymer to chloroform, thereby inducing the isomerization to cis-cisoidal segments, which are required for the subsequent cyclization and associated radical formation. This is consistent with the experimental data (Figure 2). The proposed mechanism is also consistent with the higher radical concentration in cis-cisoid-rich insoluble fractions, compared with soluble fractions, when both have been aged in the solid state. Clearly, the isomerization to the cis-cisoid structure will become increasingly difficult upon solvent evaporation and upon formation of an increasing amount of rigid cis-cisoidal segments.

The physical picture given above has been formulated into a kinetic model to describe the evolution of N_s with time. Assuming first-order kinetics for the stress-induced cyclization reaction, we can represent the time evolution of the radical concentration, $N_{\Delta E}(t)$, resulting from all sites requiring an activation ΔE for cyclization by

$$N_{\Delta E}(t) = N_{\Delta E}^{\infty}[1 - \exp(-k_0 t e^{-\Delta E/kT})] \qquad (2)$$

where the pre-exponential k_0 is assumed to be independent of ΔE and T is the absolute temperature. The maximum radical concentration $N_{\Delta E}^{\infty}$ depends on the initial distribution of strained sites, $S(\Delta E)$, which we assume is of the form

$$\frac{S(\Delta E)}{S_T} = \frac{1}{mkT}\exp\left(\frac{-\xi + \Delta E}{mkT}\right) \qquad (3)$$

where ξ is taken to be the activation energy of the unstrained cis-cisoid configuration and S_T is the total

concentration of strained sites. The total spin concentration is then given by

$$N_s(t) = \frac{N_s^\infty}{mkT}\int_0^\xi \exp\left(\frac{-\xi + \Delta E}{mkT}\right)[1 - \exp(-k_0 t e^{-\Delta E/kT})]\, d\Delta E \quad (4)$$

Best-fit curves of this function to the data of Figure 2 are given by the solid lines; the agreement is quite good.

The extent of delocalization of the cyclic π-radical, which must be considered in accounting for the partly resolved hyperfine structure of the ESR signal, depends on several factors. The most important of these is the degree of planarity of the chain in which the radical resides, the π-orbital overlap between adjacent monomer units being approximately proportional to $\cos^2\theta$, where θ is the dihedral angle between these units. For soluble samples containing a low concentration of long cis-cisoid sequences, the plane of the cyclohexadienyl ring is likely to be in coincidence with the plane of the continuing chain, thus enabling delocalization of the ring radical down the chain. The insoluble fraction would be expected to contain considerably more radicals that are trapped within the cyclohexadienyl ring, due to the lack of the planarity of the cis-cisoidal helical structure. Consequently, there is a large spin density at the carbons bonded to the two ring hydrogens. These hydrogens would be expected to be responsible for the two hyperfine splittings observed for the insoluble fractions.

The hyperfine splittings obtained for the TPCH radical are proportional to the para and ortho splittings, 13.4 and 9.0 G, reported for the unphenylated cyclohexadienyl radical.[15] The reduction in the values of the splittings for the radicals in PPA can be accounted for by assuming a dihedral angle of 40° between the TPCH ring and the continuing chain.[25]

It is not difficult to visualize that within any given sample there exists a distribution of planarity mismatches as well as of down-chain delocalization lengths. These distributions, however, are thought to be fairly narrow in the samples we have studied, since the delocalization lengths, as indicated by σ_G, are similar for soluble and insoluble samples. A random distribution of dihedral angles would result in a line width intermediate between those of the soluble and insoluble signals. Previous[5,6] and the high-temperature results meet this description.

The next most important factor controlling the extent of delocalization of the π-radical is the presence of chemisorbed oxygen on the polymer. Oxygen localizes the chain radical. This imparts a small amount of s character to it. The extent to which oxygen can interact with the polymer is dependent on the factors of steric hindrance, concentration of oxidizable sites, and acidity of the liquid media in which the polymer was dissolved. Oxygen may be bound to the polymer in the form of hydroxy or hydroperoxy groups. The highest potential for reactions with oxygen occurs during the HCl/MeOH washing step of the polymerization workup. The higher concentration of "oxy" spins of the sample washed with 1 N HCl in MeOH during polymer workup rather than the usual 0.1 N HCl solution is consistent with this hypothesis. These oxy sites may also trap the hydrogen atom liberated during the chain cyclization reaction. The greatest obstacle to oxygen chemisorption appears to be the steric hindrance imposed by helical segments. This point is consistant with the low percentage of oxy spins observed in the insoluble fraction samples.

The difference in the spatial distributions of oxy spins between the soluble and insoluble fractions also manifests itself in the spin relaxation rates. If the polymer were to possess only delocalized TPCH radicals the dominant spin–lattice relaxation mechanism would be an indirect, Raman interaction with the phonon distribution of the polymer, an inherently slow and ineffective process.[17] Spin–spin interactions would be dominated by dipole–dipole interactions, which are concentration dependent. Heisenberg spin exchange becomes important at large spin concentrations.[26] If the π-radical becomes trapped by oxygen it experiences a small increase in orbital angular momentum, resulting in a shift in the g factor, and it can therefore achieve a more intimate contact with the phonon bath.[17] As a consequence a considerable increase in the spin–lattice relaxation rate is attained. If Heisenberg spin exchange becomes important, as is the case for polyacetylene,[27] only a single spin–lattice relaxation time would be observed and consequently a unimodal saturation curve, since all the spins would be strongly coupled. For weak coupling the effects of both relaxation processes should be observable, leading to a bimodal saturation curve. The insoluble polymer contains large regions of crystalline material that are devoid of oxygen-trapped spins. Consequently the two spin systems become decoupled. The two modes of the saturation curves for the insoluble fractions are generally more separated than for the soluble fractions, in agreement with a picture of more uniform spatial distribution of oxy radicals over the latter, quasi-planar polymer.

As a sample ages the strained configurations decrease and radical formation slows due to a relaxation of the polymer chains into lower energy, stable configurations. The distribution of dihedral angles will broaden as structures experiencing less stress, requiring larger activation energies for reaction, cyclize. The net result is a decrease in spin density in the TPCH rings of crystalline samples and a larger percentage of nonplanar radicals in amorphous samples. As more spin density enters unhindered, quasi-planar chain segments, the probability of oxygen trapping increases. However, since there must be a fixed concentration of chemisorbed oxygen for a given evacuated sample, the fraction of oxygen-trapped radicals is expected to decrease. This whole process can be accelerated by heating the sample. The creation of radicals by chain cyclization ceases to occur at temperatures above 120 °C since cis-cisoid structures cannot survive above this temperature. The latter result was demonstrated by a fluorescence spectroscopy study.[4] At high temperatures the presence of oxygen is thought to lead to sample degradation, possibly resulting in decreases in spin concentration. In the absence of appreciable quantities of oxygen the structure of the polymer just continues to relax, resulting in a random distribution of planarities and delocalization lengths.

Conclusions

It has been shown that PPA/Fe–Al is a complex organometallic system rich in a variety of paramagnetic centers. The line-shape and saturation treatment of paper 1 was effectively employed to deconvolute the ESR spectra of this polymer and to enable the identification of the major chain radical as a triphenylcyclohexadienyl radical. The concentration of this species increases irreversibly in the solid state due to cyclization reactions of strained cis-cisoid 1,3,5-hexatriene segments, which result from rapid diluent volatilization in films and powders cast from solution or suspension. In addition the concentration of chain radicals complexed by oxygen was determined. These are thought to play a role in the thermal degradation of the polymer at temperatures above 100 °C.

Acknowledgment. A.L. gratefully acknowledges support by the National Science Foundation through an NSF predoctoral fellowship. This research was also supported by NSF Grant DMR-7916912 and by the SUNY-Buffalo Center for Electronic and Electro-optic Materials.

References and Notes

(1) Kern, R. J. *J. Polym. Sci., Polym. Chem. Ed., Part A-1* **1969**, *7*, 621.
(2) Ehrlich, P.; Anderson, W. A. In *Handbook of Conducting Polymers*; Skotheim, T. A., Ed.; Marcel Dekker: New York, 1986; Vol. I, p 441.
(3) Bloor, D. *Chem. Phys. Lett.* **1976**, *43*, 270.
(4) Sanford, T. J.; Allendoerfer, R. D.; Kang, E. T.; Ehrlich, P. *J. Polym. Sci., Phys. Ed.* **1980**, *18*, 2277.
(5) Holob, G. M.; Ehrlich, P.; Allendoerfer, R. D. *Macromolecules* **1972**, *5*, 569.
(6) Whitte, W. M.; Kang, E. T.; Ehrlich, P.; Carroll, J. B., Jr.; Allendoerfer, R. D. *J. Polym. Sci., Chem. Ed.* **1981**, *19*, 1011.
(7) Langner, A.; Ehrlich, P. *J. Electrochem. Soc., Extended Abstr.* **1985**, *85-1*, 124.
(8) Langner, A.; Ehrlich, P. *Synth. Met.* **1987**, *17*, 419.
(9) Simionescu, C. I.; Percec, V.; Dumitrescu, S. *J. Polym. Sci., Polym. Phys. Ed.* **1977**, *15*, 2497. Simionescu, C. I.; Percec, V. *J. Polym. Sci., Polym. Chem. Ed.* **1980**, *18*, 147.
(10) Langner, A. Ph.D. Thesis, SUNY-Buffalo, 1988.
(11) Poole, C. P. *Electron Spin Resonance, a Comprehensive Treatise on Experimental Techniques*; Wiley Interscience: New York, 1983.
(12) Singer, L. S.; Smith, W. H.; Wagoner, G. *Rev. Sci. Instrum.* **1961**, *32*, 213.
(13) Sanford, T. J.; Allendoerfer, R. D.; Schaefer, J.; Ehrlich, P. *J. Polym. Sci., Phys. Ed.* **1981**, *19*, 1151.
(14) Kang, E. T.; Langner, A.; Ehrlich, P. *Polym. Prepr. (Am. Chem. Soc., Div. Polym. Chem.)* **1982**, *23* (1), 103.
(15) Ayscough, P. B. *Electron Spin Resonance in Chemistry*; Methuen and Co.: London, 1967.
(16) Bloor, J. *Ziegler-Natta Catalysts and Polymerizations*; Academic Press: New York, 1979.
(17) Abragam, A.; Bleaney, B. *Electron Paramagnetic Resonance of Transition Ions*; Clarendon Press: Oxford, 1970.
(18) Symmons, H. F.; Boyle, G. *Proc. Phys. Soc.* **1963**, *82*, 412.
(19) Sands, R. H. *Phys. Rev.* **1955**, *99*, 1222.
(20) Castner, T., Jr.; Newell, C. S.; Holton, W. C.; Slichter, C. P. *J. Chem. Phys.* **1960**, *32*, 668.
(21) Hall, T. P. P.; Hayes, W.; Stevenson, R. W. H.; Wilkins, J. *J. Chem. Phys.* **1963**, *39*, 35.
(22) Bramley, R.; Strach, S. J. *Chem. Phys. Lett.* **1981**, *29*, 183.
(23) Owen, J.; Taylor, D. R. *J. Appl. Phys.* **1968**, *39*, 791.
(24) Simionescu, C. I.; Percec, V. *Progr. Polym. Sci.* **1982**, *8*, 133.
(25) Langner, A., unpublished results.
(26) Grant, W. J. C.; Strandburg, M. W. F. *Phys. Rev.* **1964**, *135*, A715.
(27) Dalton, L. R., private communication.

Energy Transfer in Restricted Dimensions: A New Approach to Latex Morphology[1]

Önder Pekcan,[2a] Luke S. Egan,[2b] and Mitchell A. Winnik*

Department of Chemistry, and Erindale College, University of Toronto, Toronto, Ontario, Canada M5S 1A1

Melvin D. Croucher

Xerox Research Centre of Canada, 2660 Speakman Drive, Mississauga, Ontario, Canada L5K 2L1. *Received July 27, 1989; Revised Manuscript Received November 6, 1989*

ABSTRACT: Poly(vinyl acetate) [PVAc] particles were prepared by dispersion polymerization in isooctane using a copolymer of 2-ethylhexyl methacrylate [EHMA] and 2-isocyanatoethyl methacrylate as a steric stabilizer. These reactive particles were treated with 2-(1-naphthyl)ethanol and with 2-(9-anthryl)ethanol to produce particles singly or doubly labeled specifically in the stabilizer phase. Energy transfer experiments were carried out first on the N-labeled particles doped with a hydrocarbon-soluble anthracene derivative which dissolved exclusively in the rubbery PEHMA phase and also on the doubly labeled particles. Donor fluorescence decay profiles were measured, and the data were fitted to the Klafter-Blumen model for energy transfer on fractal surfaces. The finding that the effective dimensionally $\bar{d} = 2$ for this energy transfer process is interpreted in terms of a crossover in a restricted geometry: the PEHMA domains in this material are characterized by at least one linear dimension that is small and on the order of the R_0 value (26 Å) for the energy transfer. In support of this idea, we find that swelling agents for PEHMA cause the $\bar{d}$ found in the experiments to increase systematically from 2 to 3.

Introduction

In a conventional chemical reaction, where mixing of the reactants is rapid compared to the rate of reaction, the kinetic description of the system takes a simple and familiar form.[3] In rigid media such as glasses, reaction kinetics are more complicated, particularly if the rate of reaction between any pair of reactants depends upon their separation (r) and mutual orientation (θ). Examples of these types of reactions include nonradiative energy transfer [$k_{ET}(r,\theta) \approx r^{-6}$] and electron transfer [$k_{et} \approx \exp(-\alpha r)$]. Nevertheless, when the space containing the reactants is very much larger than the distance over which the reaction takes place, the kinetics assume a familiar form, and the simplicity of the kinetic description derives from an integration of the reaction rate over the distribution of reactants over all space, i.e. $0 \leq r \leq \infty$. These ideas have been extended to reactions in two dimensions[4] and, more recently, to reactions on fractal structures.[5]

* To whom correspondence should be addressed.

0024-9297/90/2223-2210$02.50/0